HIGHER-ORDER MODE CALCULATIONS, PREDICTIONS AND OVERVIEW OF DAMPING SCHEMES FOR ENERGY RECOVERING LINACS*

R.A. Rimmer

Jefferson Lab, 12000 Jefferson Ave, Newport News, VA 23606, USA

Corresponding author: Robert Rimmer

Jefferson Laboratory

12000 Jefferson Avenue

Newport News, VA 23606, USA

Phone: 757-269-7375

FAX: 757-269-7658

email: rarimmer@jlab.org

ABSTRACT

This paper gives a brief review of computational methods for calculating higher-order mode (HOM) impedances for RF structures, the cases for which they are appropriate and some comparisons with measurements. An overview of damping schemes suitable for moderate to high current energy recovered linacs (ERL's), is presented, with a discussion of the pro's and con's of each. The influence of number of cells per cavity, cell shape and cell-to-cell coupling are described. The Jefferson Lab Ampere-class cryomodule concept is presented as an example and the issue of HOM power is highlighted.

Keywords: RF; HOM; ERL

*This manuscript has been authored by SURA, Inc. under Contract No. DE-AC05-84ER-40150 with the U.S. Department of Energy, and by The Office of Naval Research under contract to the Dept. of Energy.

1. INTRODUCTION

High average power ERL's proposed for free electron lasers and other light source applications face many of the same challenges as storage ring light sources and high-luminosity electron-positron colliders. In particular beam instabilities caused by cavity higher-order modes (HOMs) may limit the maximum sustainable current and therefore optical power. Thankfully the situation is somewhat easier to treat in ERL's due to the fact that each bunch spends a relatively short time in the machine, however beam break up (BBU) can occur if the impedances of the cavity HOMs are not sufficiently reduced. The next generation of "industrial-strength" FEL's may have parameters requiring energies of greater than 100 MeV, beam currents exceeding 100 mA and optical power output in excess of 100kW. Such machines will require strong damping of cavity HOMs and careful handling of the beam-induced HOM power.

2. METHODS OF HOM CALCULATION

One of the first methods adopted for calculating the external coupling to HOMs using aperture or waveguide dampers was the Kroll-Yu or Kroll-Lin method [1,2]. This is a perturbation technique in which the resonant modes of a cavity system are calculated for various lengths of damping waveguide with non-absorbing boundaries. A numerical model such as that in Figure 1 could be used to calculate all the modes up to some limit set by computer size or run time. By tracking the cavity and waveguide resonances and seeing where they intersect and how strongly they interact it is possible to extract the coupling constant for a particular mode. This is achieved by a numerical fit to the curves in the "avoided crossing" regions. This method works best for very strong coupling ($B>>1$) but requires a lot of computer runs.

A more versatile method is to take advantage of codes which can simulate beam-induced wakefields in the time domain, such as ABCI [3], (2D), and MAFIA [4],(3D). In this case a numerical model can be excited by the passage of a simulated bunch that is short enough to contain current components up to the highest frequency of interest, and can have open "absorbtive" or "radiative" boundary conditions on one or more ports, figure 3. By recording the long-range wakefield for a long distance behind the bunch and then taking the Fourier transform the broad-band impedance can be calculated directly. Figure 4 shows the short, medium, and long-range wakes calculated in this way. The frequency resolution of the spectrum is set by the length of the time record, while the minimum time step is determined by the upper frequency and the frequency content of the simulated bunch. This method is computationally efficient, typically requiring just two runs to get all the longitudinal and transverse modes below the beam-pipe cut-off. This method has been checked against bench and beam-based measurements [5]. Figure 5 shows a comparison with bead-pull data for a single-cell cavity for PEP-II. Figure 6 shows the beam-induced signal coming out one of the HOM ports (top) versus the calculated spectrum (bottom). The method works best for strong coupling and for frequencies up to about 10 GHz (limited by mesh size and computer speed).

Other methods include growth and decay methods [6], in which a shorter time record is required and a cavity mode is either excited by a signal, figure 7, or pre-loaded and allowed to decay, figure 8. In either case the time response of the cavity amplitude and/or signals or energy flow in external ports can be used to quantify the Qext of the system. These methods can be used for systems with higher Q's but at least one run is needed for each mode of interest.

For very high Q's such as may be found in superconducting cavities (e.g. 10^6-10^{10}), a perturbation method may be employed, using the frequency difference between open and short terminations [7].

Direct complex Eigenvalue solution is now becoming available in codes such as HFSS [8], figure 9, and Omega [9]. In this case the real and imaginary parts of impedance are calculated directly, and hence R and Q can be derived. Note the traveling-wave component in the beam pipes in figure 9.

3. METHODS OF BROAD-BAND HOM DAMPING

Strong HOM damping has been demonstrated in various single-cell cavities, e.g. Cornell, KEK and SLAC B-factory storage rings. Studies show these methods can be also be applied to multi-cell cavities [10]. Options include using multiple coaxial antennas, enlarged or fluted beam pipes, waveguide dampers, and coaxial beam-pipes, see figures 10a-e. The waveguide and beam-pipe (round waveguide) methods use a length of cut-off waveguide to reject the accelerating mode while the coaxial and radial dampers require a choke or notch filter to reject the fundamental. Numerical analysis of each of these methods (except the multiple coax solution which is difficult to simulate and has been widely used already), on a single-cell shows that they all give excellent damping, as expected, see figure 11 and table 1. The beam-pipe loaded methods give very strong damping but in practice give up some active length to accommodate the evanescent decay of the fundamental mode, the cold to warm transition and the absorber itself (which is also exposed to the beam). The waveguide-loaded method also gives good damping while using less than one cell-length of beam-pipe real estate, resulting in a higher overall effective gradient. The coaxial beam pipe, if coupled to a radial damper could also provide a compact solution but requires a superconducting choke in series to block the fundamental. Similarly good performance can be achieved for transverse modes in all cases.

To study the effectiveness of the broad-band damping on multi-cell cavities as a function of the number of cells one method (beam-pipe damping), was applied to models with from one to

seven cells. As can be seen in figures 12 through 15 the Q's and impedances degrade as more cells are added. For the TM110 (dipole) mode there is an interesting bifurcation in the Q's between odd and even numbers of cells, however the resulting impedance still increases monotonically as the number of cells is increased. After a jump between one and two cells the impedance only increases slightly faster than linearly with number of cells and cavities with as many as five or six cells look to be a reasonable proposition for high-current ERL applications. Existing JLab infrastructure is compatible with 5-cell cavities at 750 MHz, providing the beam-pipes are not too long.

Another consideration is the effect of cell shape or cell to cell coupling on the damping performance. To study this we compared 7-cell cavities of three different shapes with the same beam-pipe damping. As can be seen in figures 16 and 17 the mode spectra of the cavities can be quite different but the worst-case modes are of similar strength in each case. The differences in mode frequencies may however be very important in determining the BBU threshold and HOM power dissipated by the loads. Tables 2 and 3 list the strongest monopole and dipole modes in each pass-band below cut-off as well as a waveguide-damped 5-cell cavity (with CEBAF cell shape), and coaxially damped 4-cell (HERA) cavity for comparison.

4. EXAMPLES

An example of a strongly damped multi-cell cavity with beam-pipe damping is the BNL concept for electron cooling at RHIC, figure 18 [11]. In this case real-estate gradient is not important and they can take advantage of the high-power ferrite loads developed at Cornell. An example of waveguide damping is the JLab Ampere-class cryomodule under development for compact high-power FEL's [12]. Table 4 shows the draft requirements of such a module and figure 19 shows a cavity concept that looks promising to meet or exceed those requirements. This

version has four damping waveguides symmetrically arranged on each end. This gives excellent damping and no dipole coupler kicks. Other concepts using three waveguides on each end also look promising. Comparing the monopole and dipole spectra for this waveguide-loaded cavity to those with beam-pipe damping shows the results are very similar, see figures 20 and 21. The loaded Q's and impedances of the worst modes are within the target specifications in both cases, but the real estate gradient of the waveguide-damped version is much higher.

Packaging this cavity can be accommodated within an SNS-style cryomodule. The HOM loads would be taken out to room temperature and be water cooled because of the high HOM power expected. Concepts using modified SNS couplers and also waveguide fundamental power couplers (FPC) are being developed. Figure 22 shows one such concept with a pair of coaxial FPC's arranged symmetrically. In practice one FPC is probably sufficient to provide all the power needed and the end group could be adapted to eliminate the dipole kick from a single coupler. Figure 23 shows this assembly in an SNS-style space frame. It is a tight fit because of the slightly lower frequency and added waveguide dampers but it looks achievable and this would allow reuse of much of the SNS cryomodule tooling. Table 5 shows the parameters of a cryomodule based on this concept.

5. HOM POWER

The amount of power deposited in the cavity by high-current re-circulated beams may be significant. The exact amount of power depends on the cavity mode spectrum, level of HOM damping, bunch fill pattern(s) and recirculation path length. For most proposed ERL's (racetrack configuration), the beam is re-circulated in the same direction but at decelerating phase. This produces energy recovery at the fundamental and odd harmonics but actually results in addition at the even harmonics. Thus for a 1A DC beam figure 24, (2A RF current single pass), with every

bunch filled, there is a 4A source term at odd harmonics of the fundamental, figure 25. Since the bunch is typically very short this power spectrum may extend up to very high frequencies. Care must be taken to choose a cell shape that does not have HOMs that strongly interact with these current lines. For sparsely filled machines there are many intermediate current lines at multiples of the recirculation frequency, figure 26. The strength of these lines depends on the phase of the re-circulated beam at each frequency. Although the average current is typically much lower for sparsely populated machines it may still be problematic if a strong HOM lands on one of these current lines. Figure 27 shows the impedance spectrum of a 750 MHz five-cell cavity with the CEBAF cell profile overlaid on the beam spectrum for 1A, every bucket filled. Figure 28 shows the same with 100 mA, every 10th bucket filled.

6. CONCLUSIONS

A variety of schemes are available for HOM calculations using many different codes and many of those have been cross-checked with experimental measurements. There are several choices for strong HOM damping, and all can give good Q's. Cell shape and cell to cell coupling can influence Q's (weakly) and frequencies (strongly). High-current tends to push us to fewer cells per cavity and lower frequencies. Several high-current cryomodule concepts are being developed for FEL's, electron cooling etc. Superstructures, though not discussed here, may be a useful way to further increase real-estate gradient. HOM power may be at least as much of a concern as BBU and may be a significant factor in choosing cell shape and module configuration.

TABLES

FIGURE CAPTIONS

Figure 1. Pillbox model with waveguide damping.

Figure 2. Mode frequencies vs waveguide length.

Figure 3. Model of a cavity with open waveguides.

Figure 4. Short-, medium-, and long-range wakes.

Figure 5. Calculated vs. measures mode impedances.

Figure 6. Measured (top) and calculated (bottom) HOM signal coming out of the cavity in the ring.

Figure 7. Linear "growth" method (MAFIA)

Figure 8. Mode decay method (MAFIA)

Figure 9. HFSS 3D complex Eigenvalue solution, dipole mode, 5-cell cavity with enlarged beam-pipes.

Figure 10a. Single enlarged beam pipe

Figure 10b. Fluted beam pipe

Figure 10c. Waveguide dampers

Figure 10d. Coaxial beam pipe.

Figure 10e. Multiple coaxial loops.

Figure. 11. TM_{011} mode impedance with various damping schemes.

Figure 12. TM_{011} pass-band mode for different numbers of cells.

Figure 13. TE_{111} and TM_{110} pass-bands for different numbers of cells.

Figure 14. Loaded Q vs. number of cells, beam-pipe damping.

Figure 15. Shunt impedance, R, vs. number of cells (R @ 25mm for dipoles).

Figure 16. TM_{011} band, OC, HG, LL shapes, 7-cells, beam-pipe damping.

Figure 17. 7-cells, OC, HG, LL shapes, TE_{111}/TM_{110} dipole modes, beam-pipe damping.

Figure 18. BNL 5-cell cavity for electron cooling.

REFERENCES

[1] N. Kroll, D. Yu, "Computer Determination of the External Q and Resonant Frequency of Waveguide Loaded Cavities", Particle Accelerators, 1990, Vol. 34, pp.231-250.

[2] N. Kroll, X. Lin, "Computer Determination of the Properties of Waveguide Loaded Cavities", Proc. Linear Acc. Conf., Albuquerque, NM, Sept 10-14, 1990.

[3] Y. H. Chin, "ABCI User's Guide", Version 8.8, February, 1994. LBL-35258.

[4] X.E. Lin, K. Ko, C.-K. Ng, " Impedance Spectrum for the PEP-II RF Cavity". Proc PAC 95, Dallas, TX.

[5] R. Rimmer, J. Byrd, D. Li, "Comparison of Calculated, Measured and Beam Sampled Impedance of a HOM-damped RF Cavity", Physical Review Special Topics - Accelerators and Beams, Volume 3, 102001 (2001).

[6] D. Li , , R. Rimmer, S. Kosta, "Calculations of External Coupling to a Single Cell RF Cavity", Proc. LINAC 98, Chicago, Illinois, USA, August 23 - 28, 1998.

[7] P. Ballyguier, "A Straightforward Method for Cavity External Q Computation", Particle Accelerators, 1997, Vol. 57, pp 113-127.

[8] http://www.ansoft.com /products/hf/hfss/

[9] Liequan Lee et al., "Modeling RF Cavity with External Coupling", 2005 SIAM Conference on Computational Science and Engineering, Orlando, Florida, February 2005.

[10] R. Rimmer, H. Wang, G. Wu, "Strongly HOM-Damped Multi-cell RF Cavities for High-Current Applications", Proc. SRF03, Lubeck, Germany, 8-12 Sept 2003.

[11] I. Ben-Zvi et. al., "Extremely High Current, High-Brightness Energy Recovery Linac", Proc. PAC05, Knoxville, TN, May 16-20, 2005.

[12] R. Rimmer et. al., "Concepts for the JLab Ampere-Class CW Cryomodule", Proc PAC05, Knoxville, TN, May 16-20, 2005.

Table 1. TM_{011} mode for various damping methods.

	Freq. MHz	Qext	R* (Ω)	R/Q (Ω)
b-pipe	2803	252	3001	11.9
flutes	2803	137	1010	7.3
w-guide	2800	353	5040	14.3
bp-coax	2783	725	11879	16.4
2xbp	2822	121	1481	12.2

*$R=V^2/2P$

Table 2. TM_{011} mode data for multi-cell cavities.

	#cells	Freq,MHz	Qext	R† (Ω)	R/Q (Ω)
OC	7	2876	527	31463	59.7
HG	7	2876	1348	90380	67.0
LL	7	2629	985	53556	54.4
OC*	5	2871	707	35453	50.1
DESY	4	910	600		

*waveguide damped. **500 MHz cavity, meas. Q. †$R=V^2/2P$

Table 3. TE_{111}/TM_{110} mode data for multi-cell cavities.

	# cells	TE_{111} f, MHz	TE_{111} Qext	TE_{111} R†, (Ω)	TM_{110} f, MHz	TM_{110} Qext	TM_{110} R† (Ω)
OC	7	1922	135	6088	2099	4177	72101
HG	7	2014	185	11359	2156	5694	146409
LL	7	2021	490	14107	2209	2071	39510
OC*	5	1894	956	22949	2103	3274	47064
DESY	4	650	4000		716	6000	

*waveguide damped. †R calculated at 25mm offset in cavity.

Table 4. JLab FEL Ampere-class module draft specifications.

Voltage	100-120 MV
Length	~10m
Frequency	750 MHz
Beam Aperture	>3”
BBU Threshold	>1A
HOM Q’s	$<10^4$

Table 5. 750 MHz cryomodule with six five-cell cavities with waveguide damping.

Frequency	750 MHz
# cells	5
Damping Type	Waveguide
Cavity Length	1.4m
Iris Diameter	14 cm (5.5”)
# Cavities	6
Min. Module Length	10.4m
Nominal Module Voltage	100 MV (120 MV peak)
Cavity Gradient (Eacc)	16.7 MV/m (20 MV/m max)
Real Estate Gradient	~10 MV/m
TE_{111} freq, Qext	947 MHz, 9.5e2
TM_{110} freq, Qext	1052 MHz, 3.3e3
TM_{011} freq, Qext	1436 MHz, 7.1e2
HOM Power/Cavity	~20 kW(est)
BBU Threshold	>1A

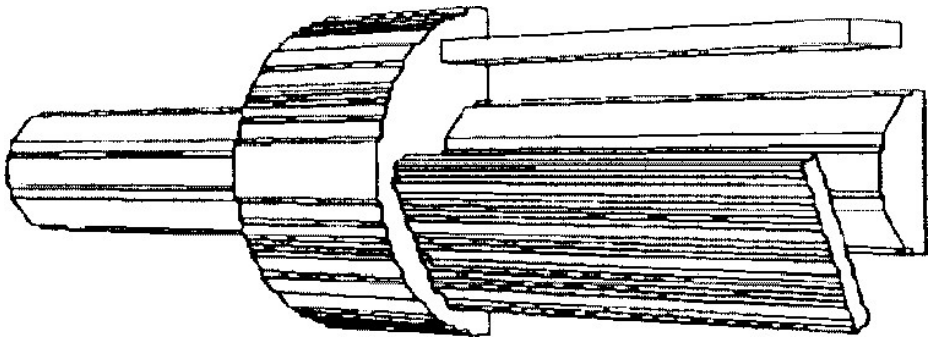

Figure 1.

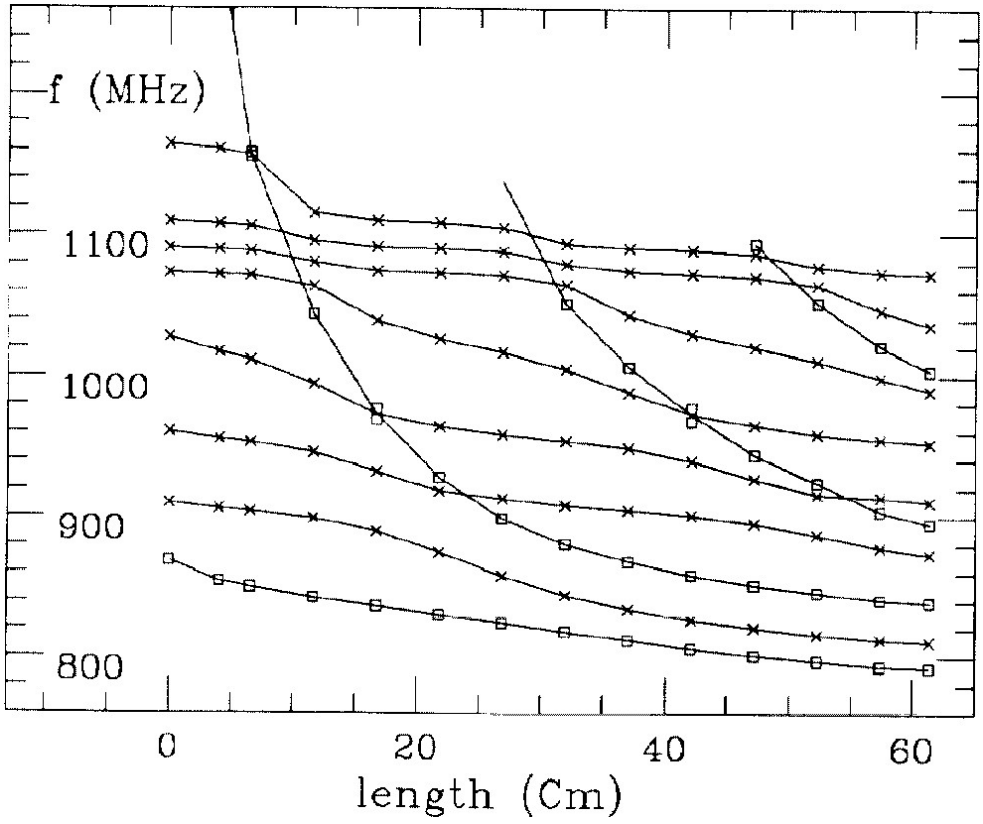

Figure 2.

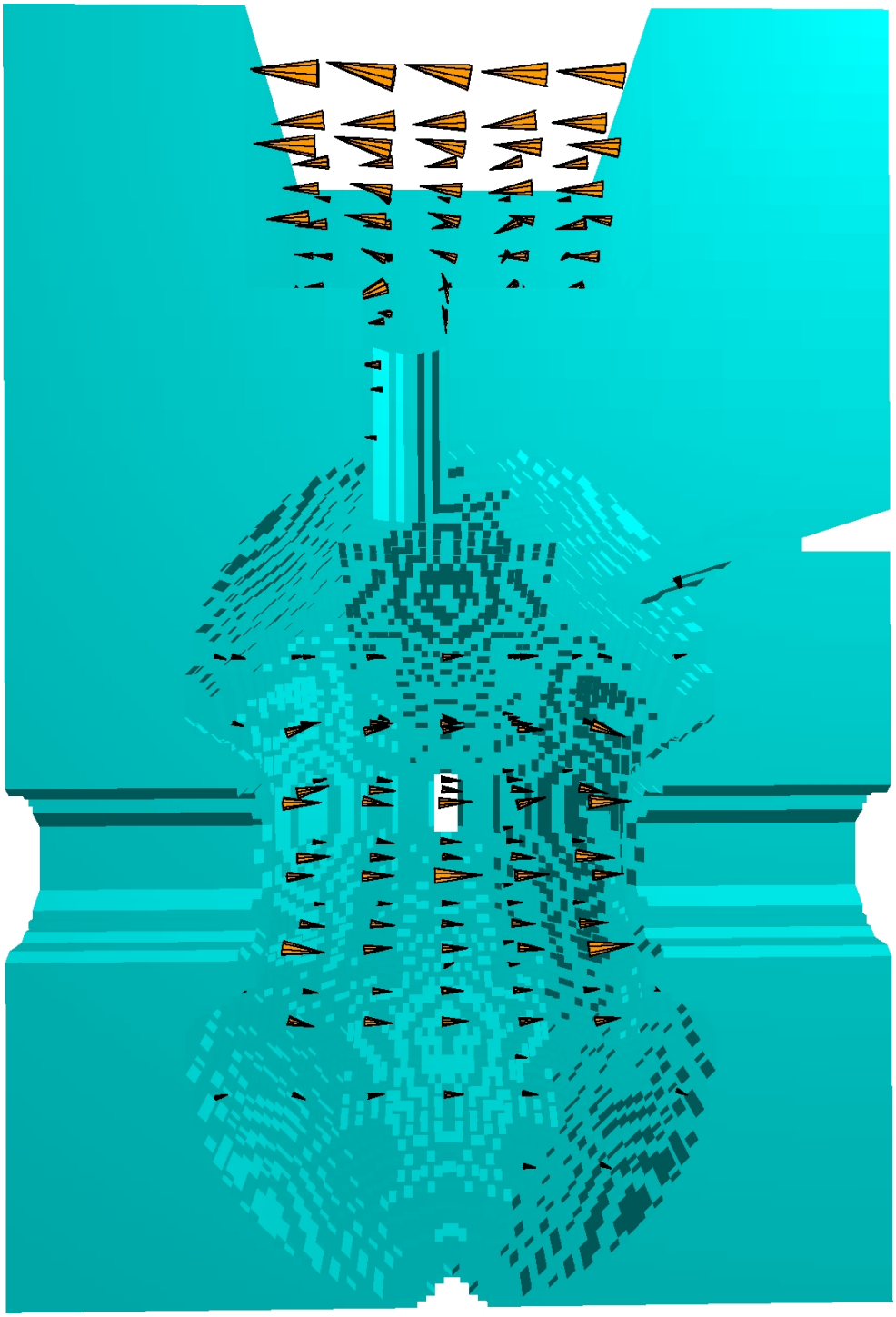

Figure 3.

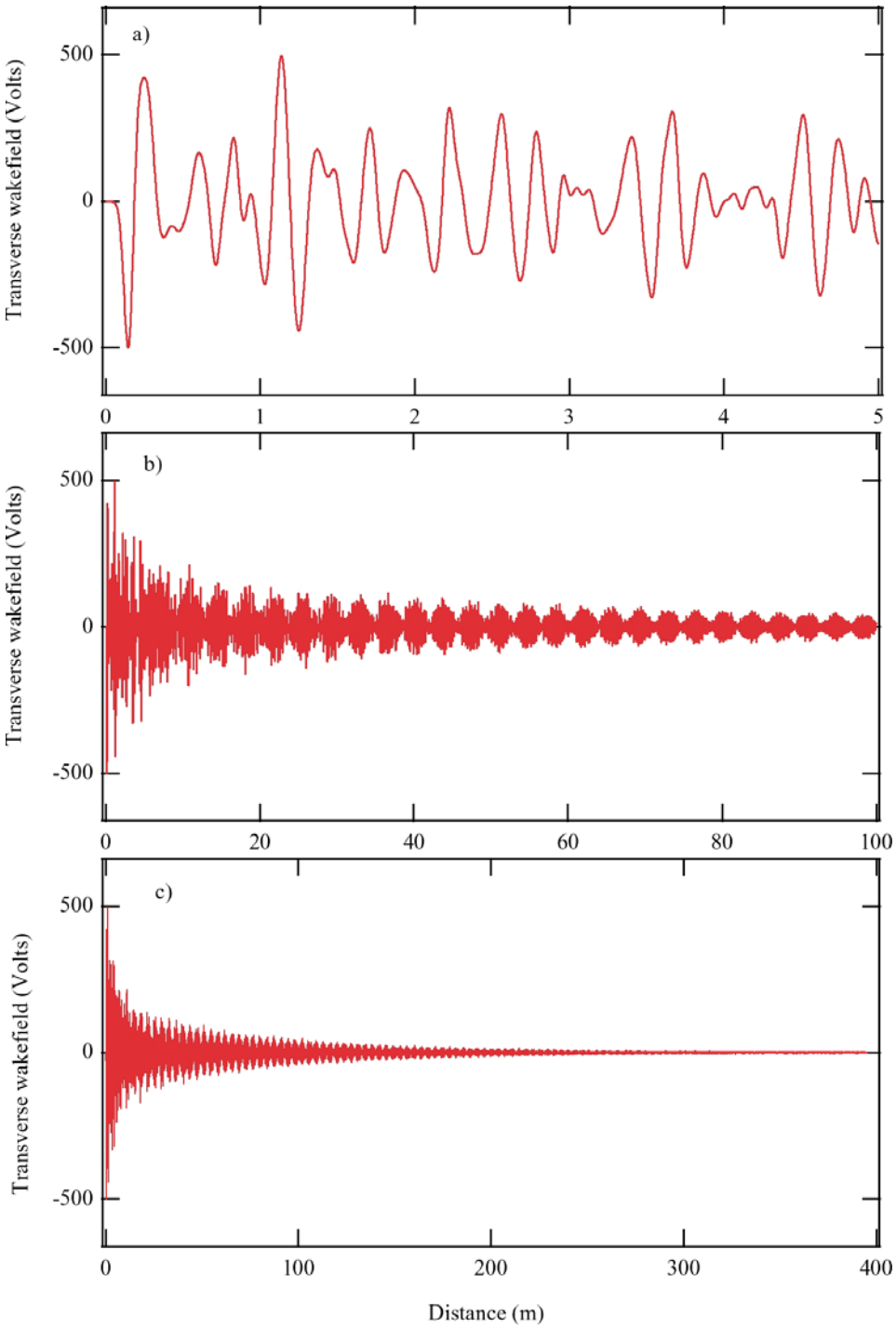
a)
b)
c)
Transverse wakefield (Volts)
500
0
-500
0
1
2
3
4
5
20
40
60
80
100
200
300
400
Distance (m)

Figure 4.

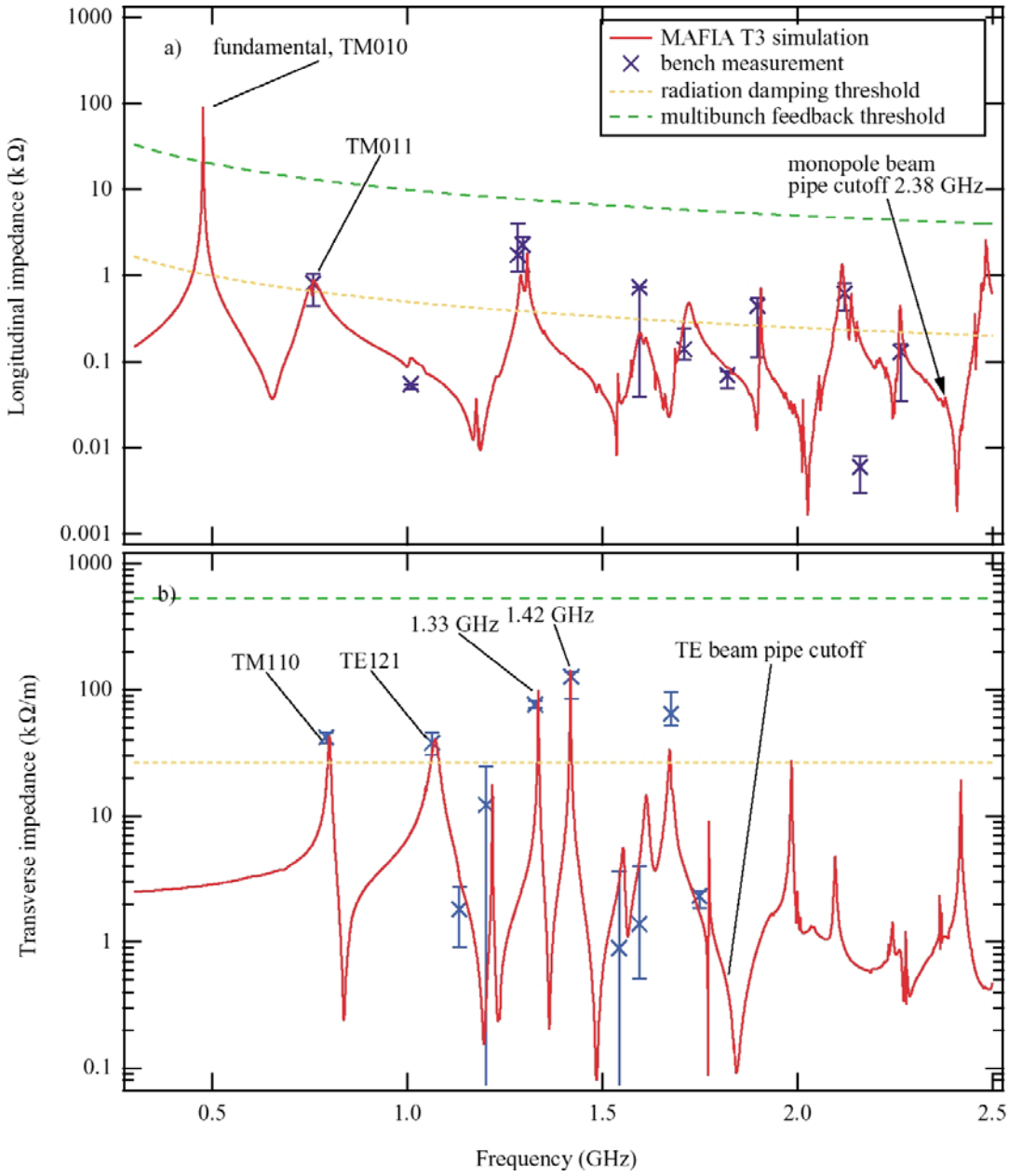
a)
fundamental, TM010
TM011
monopole beam
pipe cutoff 2.38 GHz
MAFIA T3 simulation
bench measurement
radiation damping threshold
multibunch feedback threshold
Longitudinal impedance (k Ω)
1000
100
10
1
0.1
0.01
0.001
b)
TM110
TE121
1.33 GHz
1.42 GHz
TE beam pipe cutoff
Transverse impedance (kΩ/m)
1000
100
10
1
0.1
0.5
1.0
1.5
2.0
2.5
Frequency (GHz)

Figure 5.

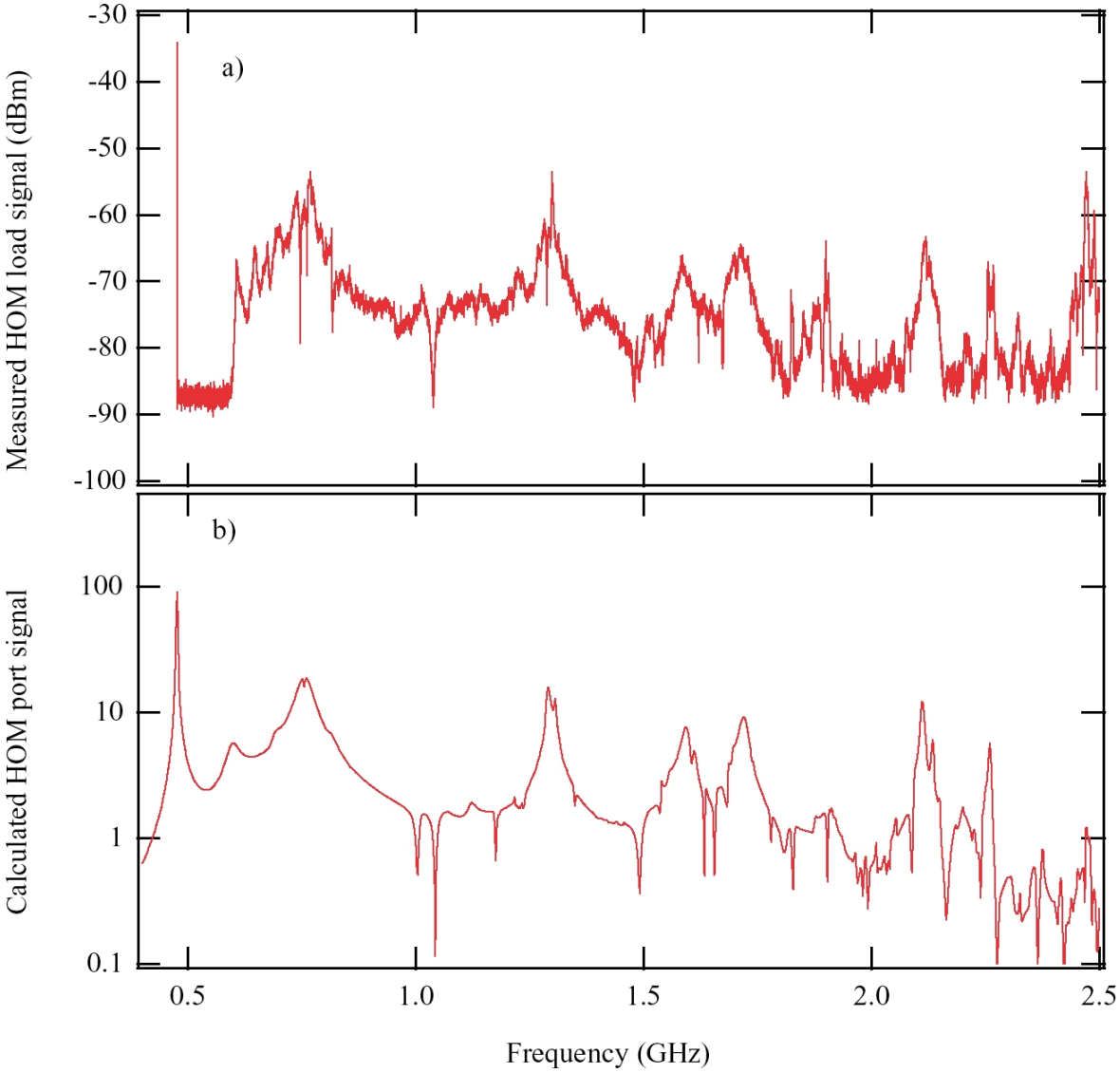
-30
-40
-50
-60
-70
-80
-90
-100
a)
Measured HOM load signal (dBm)
b)
100
10
1
0.1
Calculated HOM port signal
0.5
1.0
1.5
2.0
2.5
Frequency (GHz)

Figure 6.

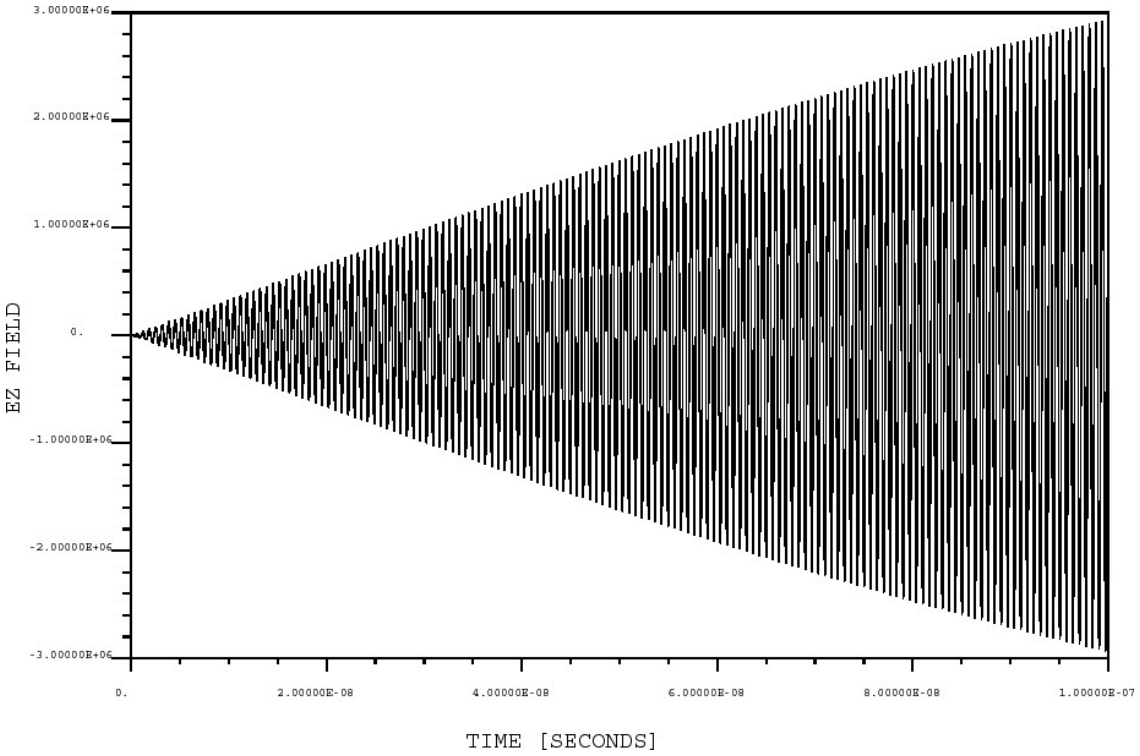
3.00000E+06
2.00000E+06
1.00000E+06
0.
-1.00000E+06
-2.00000E+06
-3.00000E+06
EZ FIELD
0.
2.00000E-08
4.00000E-08
6.00000E-08
8.00000E-08
1.00000E-07
TIME [SECONDS]

Figure 7.

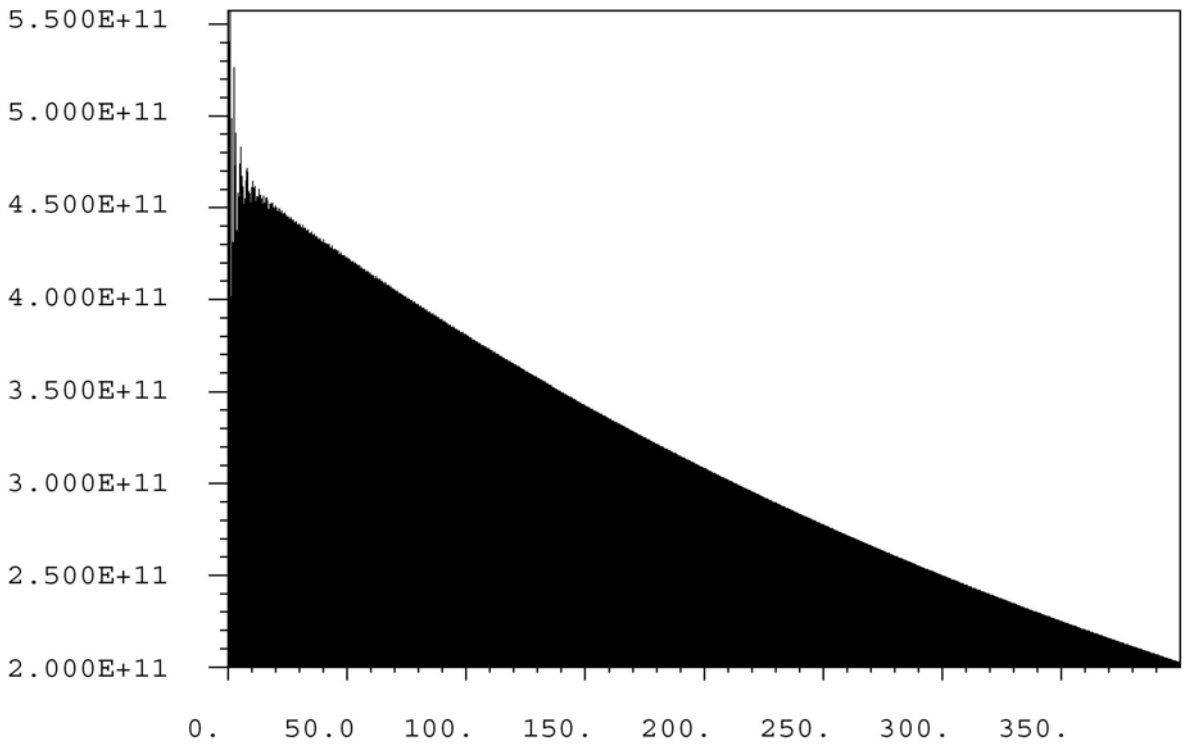
5.500E+11
5.000E+11
4.500E+11
4.000E+11
3.500E+11
3.000E+11
2.500E+11
2.000E+11
0.
50.0
100.
150.
200.
250.
300.
350.

Figure 8.

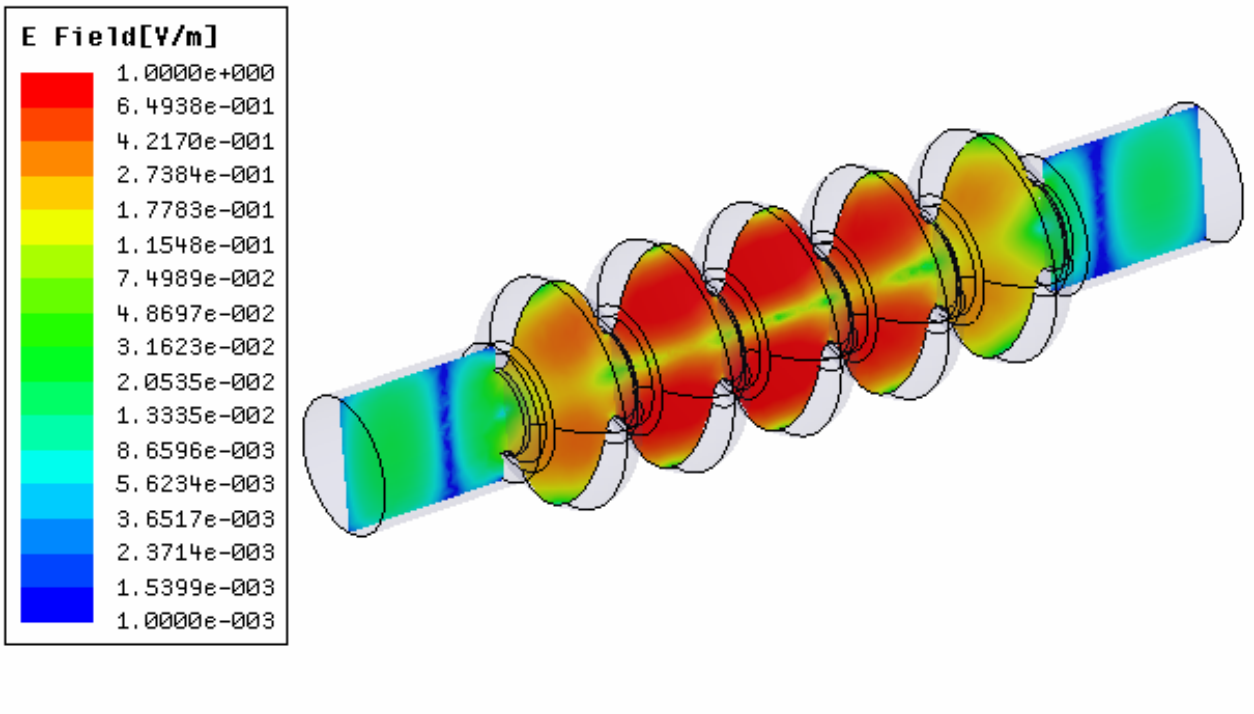
E Field[V/m]
1.0000e+000
6.4938e-001
4.2170e-001
2.7384e-001
1.7783e-001
1.1548e-001
7.4989e-002
4.8697e-002
3.1623e-002
2.0535e-002
1.3335e-002
8.6596e-003
5.6234e-003
3.6517e-003
2.3714e-003
1.5399e-003
1.0000e-003

Figure 9.

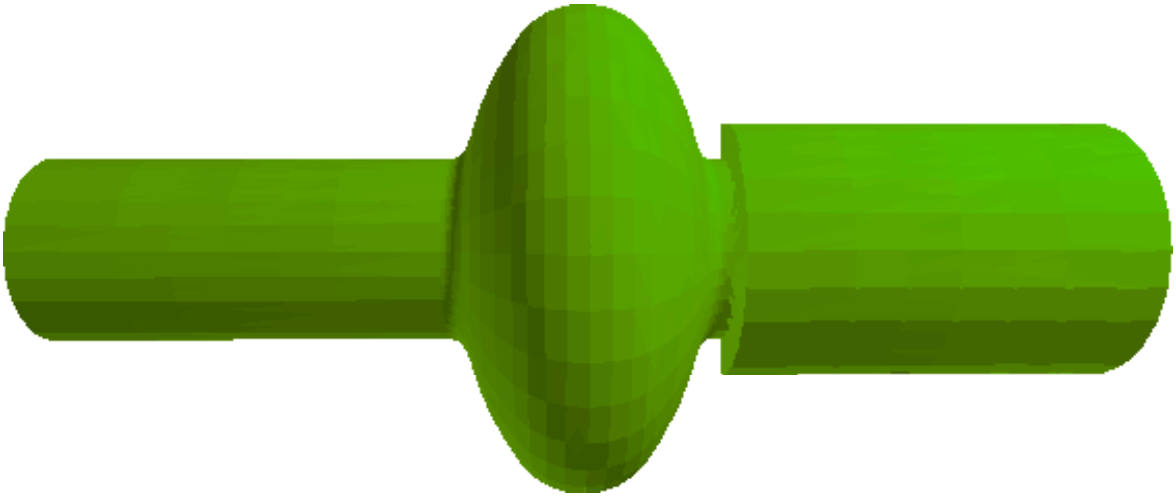

Figure 10a.

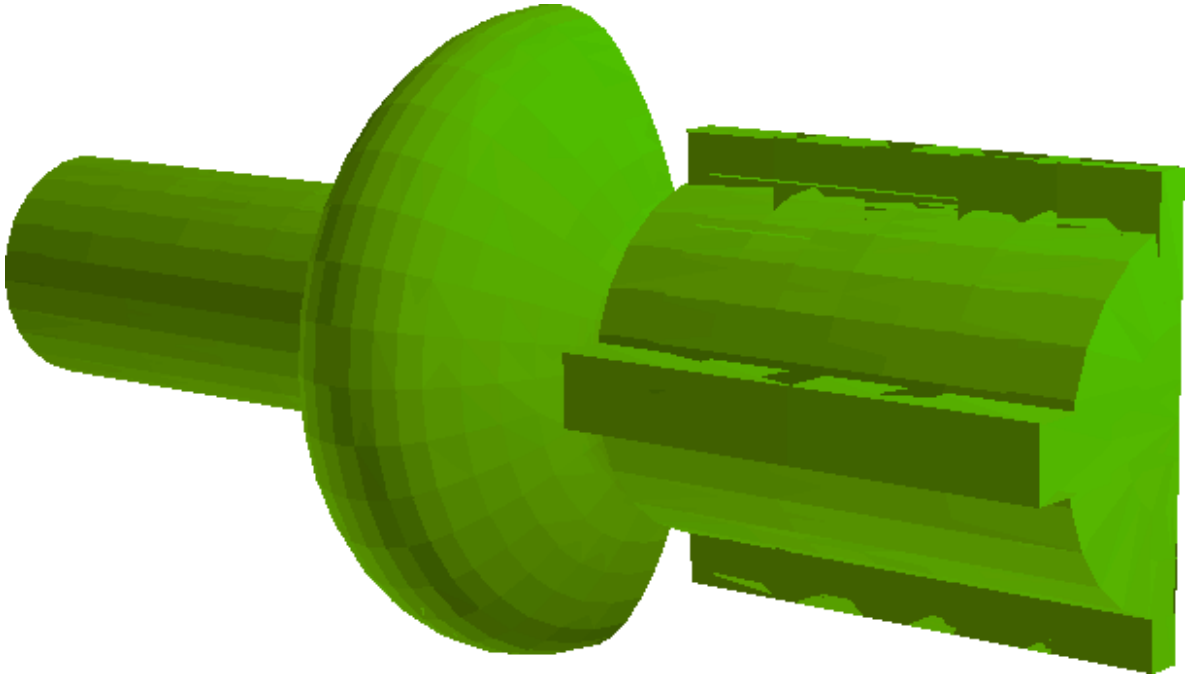

Figure 10b.

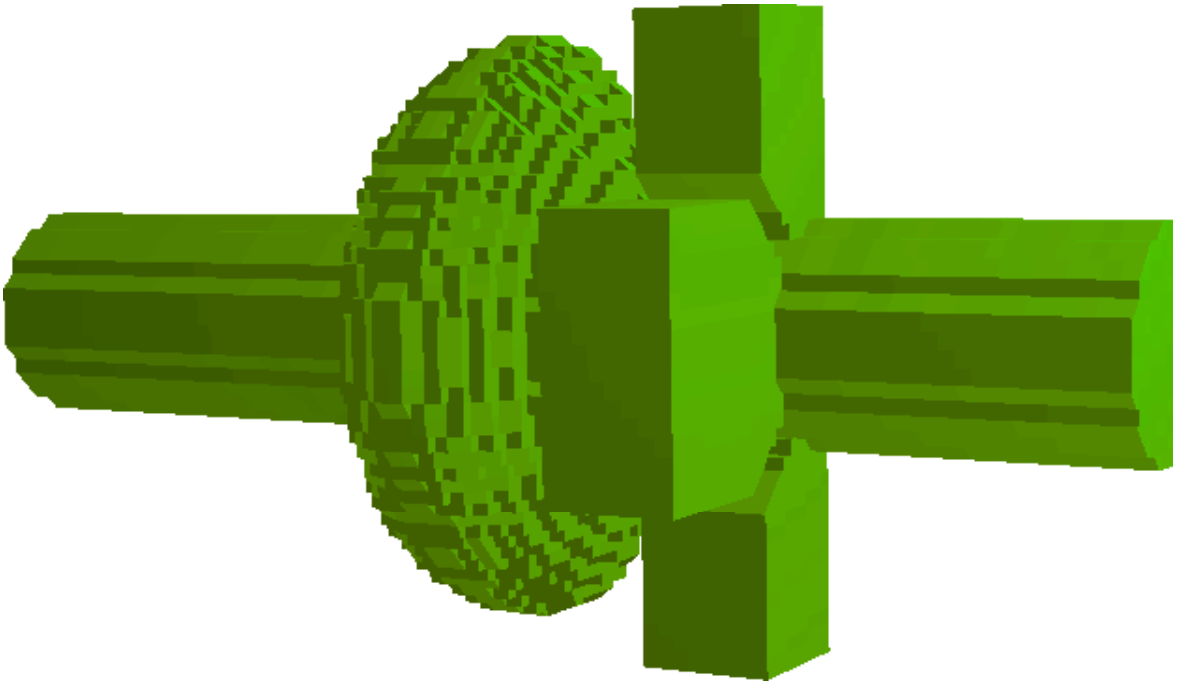

Figure 10c.

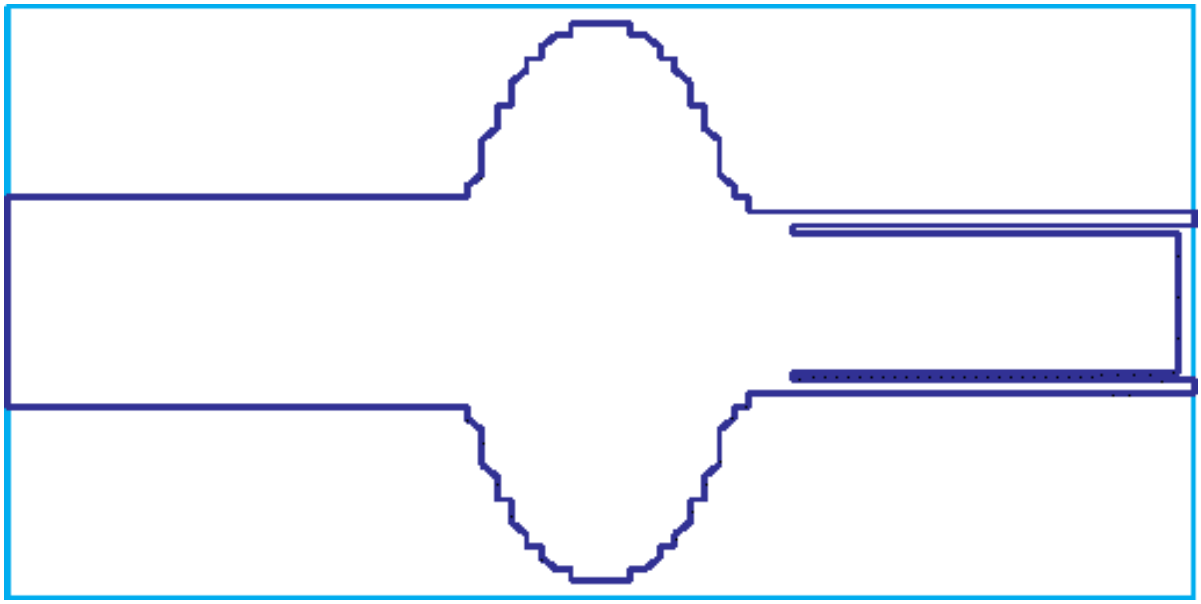

Figure 10d.

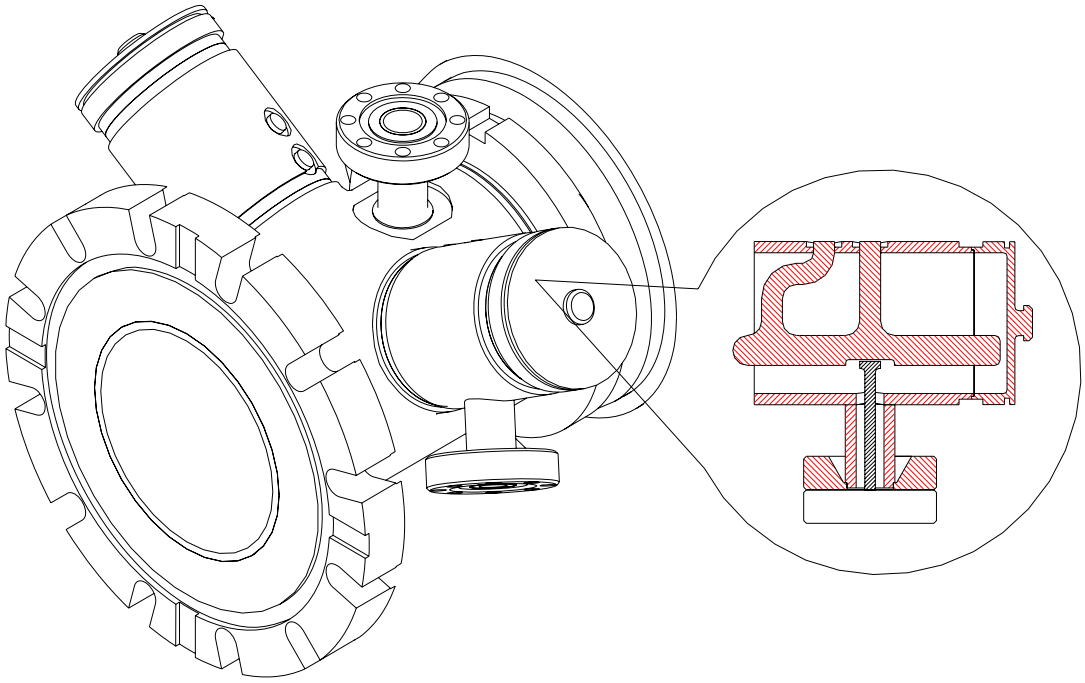

Figure 10e.

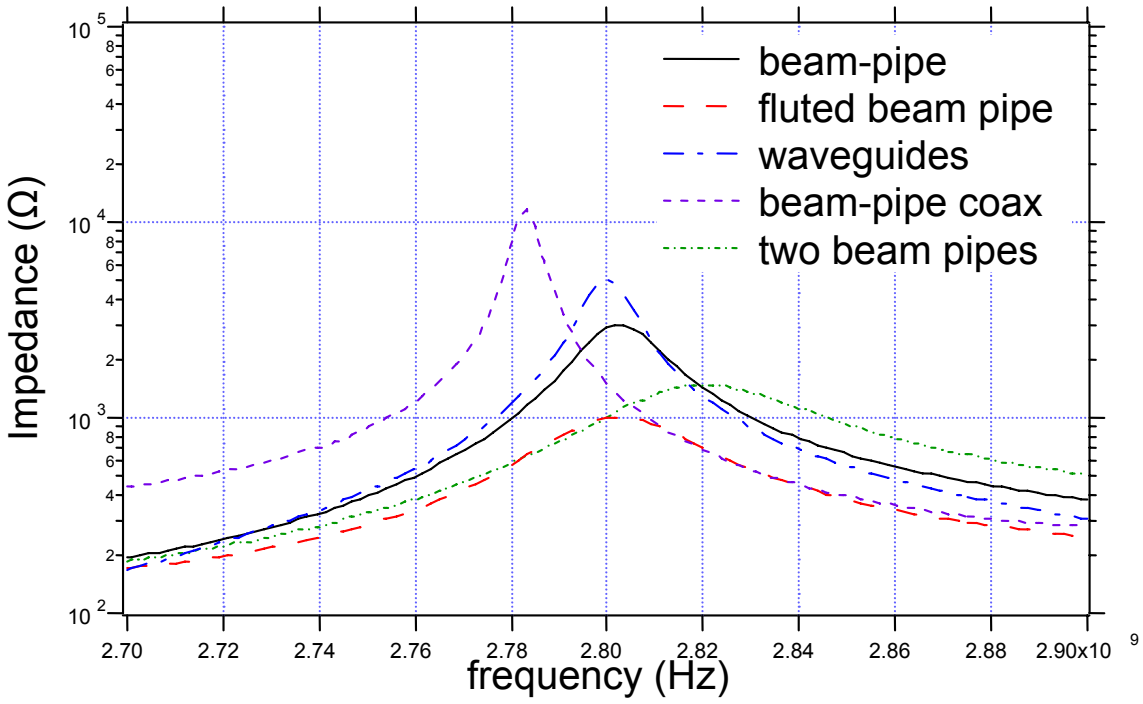
beam-pipe
fluted beam pipe
waveguides
beam-pipe coax
two beam pipes
Impedance (Ω)
frequency (Hz)
10 5
10 4
10 3
10 2
2.70
2.72
2.74
2.76
2.78
2.80
2.82
2.84
2.86
2.88
2.90x10 9

Figure. 11.

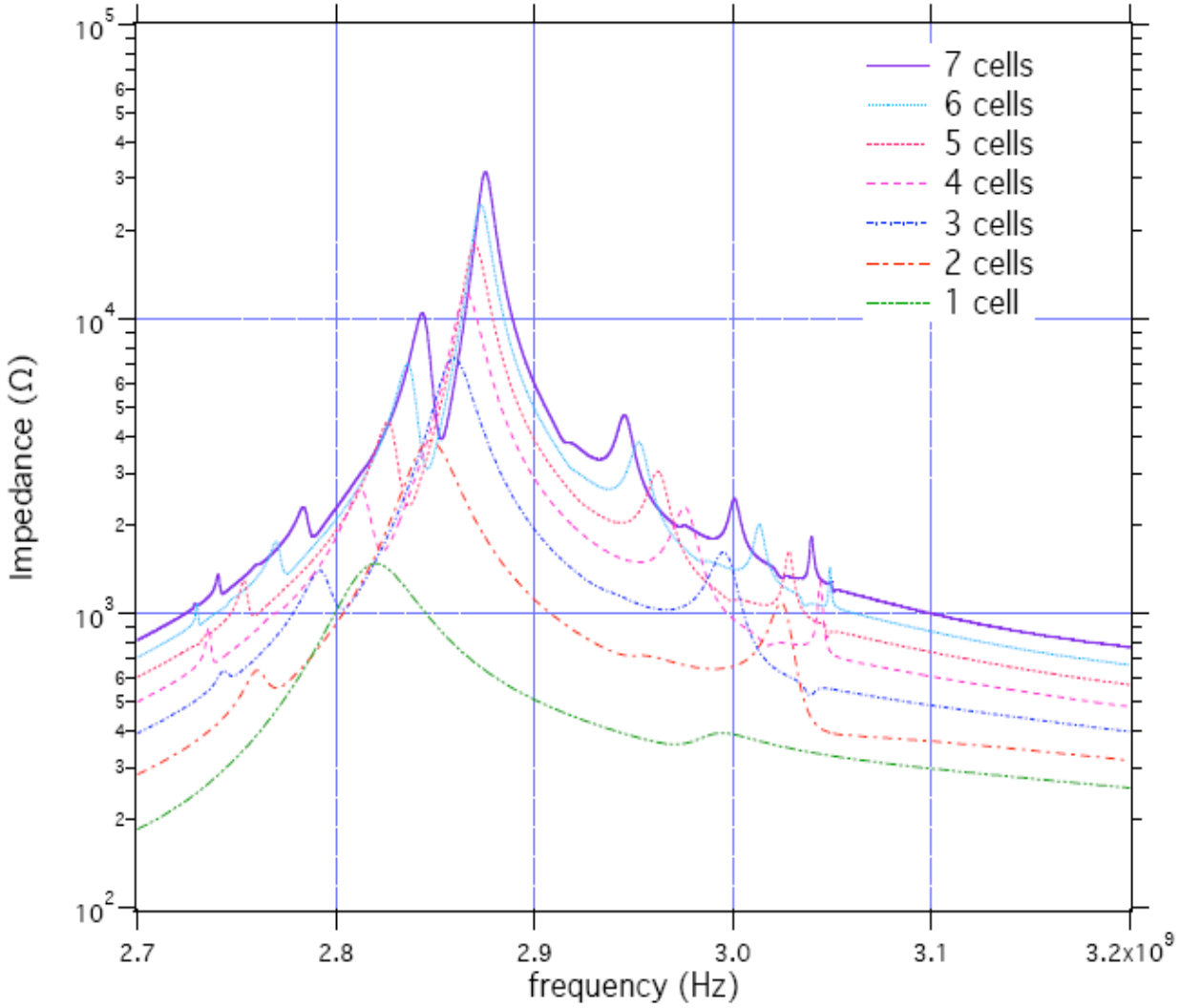
7 cells
6 cells
5 cells
4 cells
3 cells
2 cells
1 cell
Impedance (Ω)
frequency (Hz)
2.7
2.8
2.9
3.0
3.1
3.2x10^9

Figure 12.

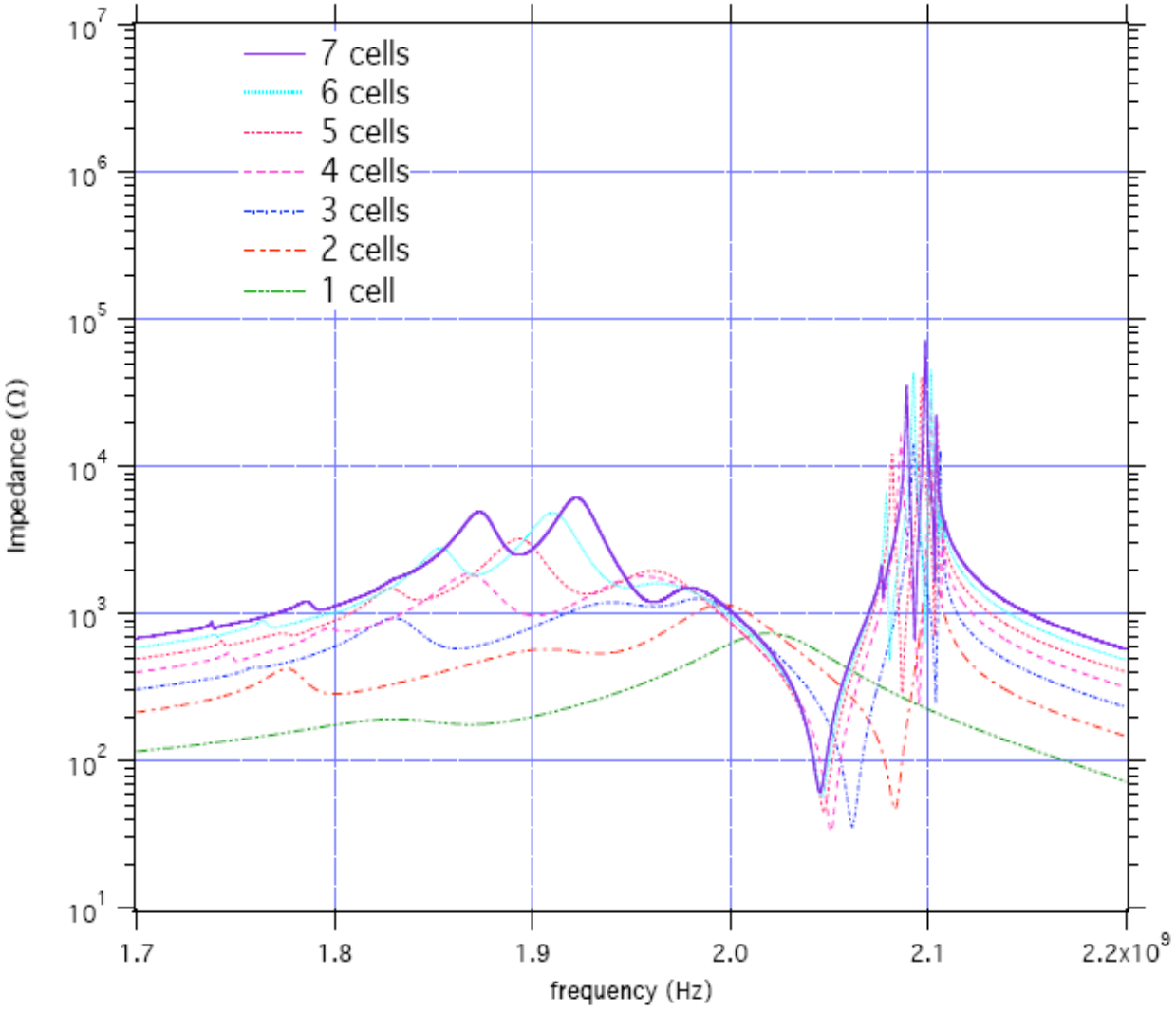
7 cells
6 cells
5 cells
4 cells
3 cells
2 cells
1 cell
Impedance (Ω)
frequency (Hz)
1.7
1.8
1.9
2.0
2.1
2.2x10^9

Figure 13.

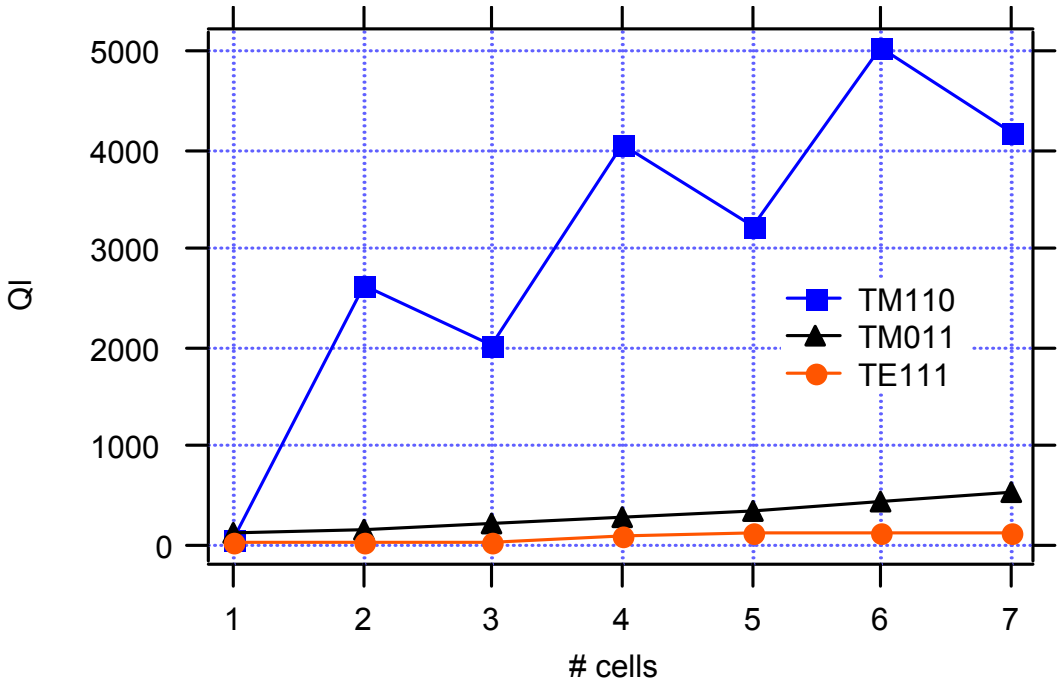
5000
4000
3000
2000
1000
0
QI
1
2
3
4
5
6
7
cells
TM110
TM011
TE111

Figure 14.

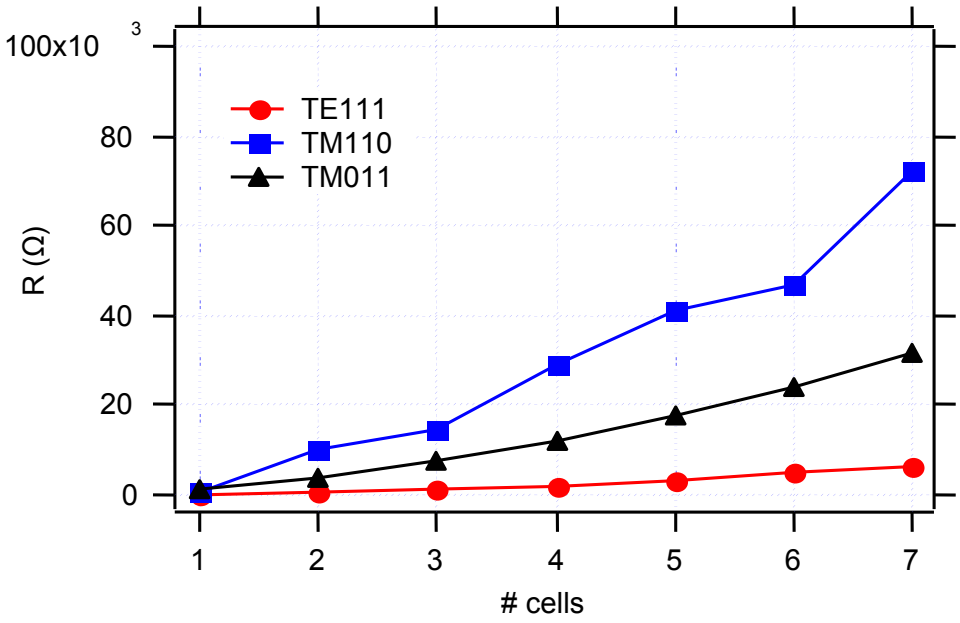

Figure 15.

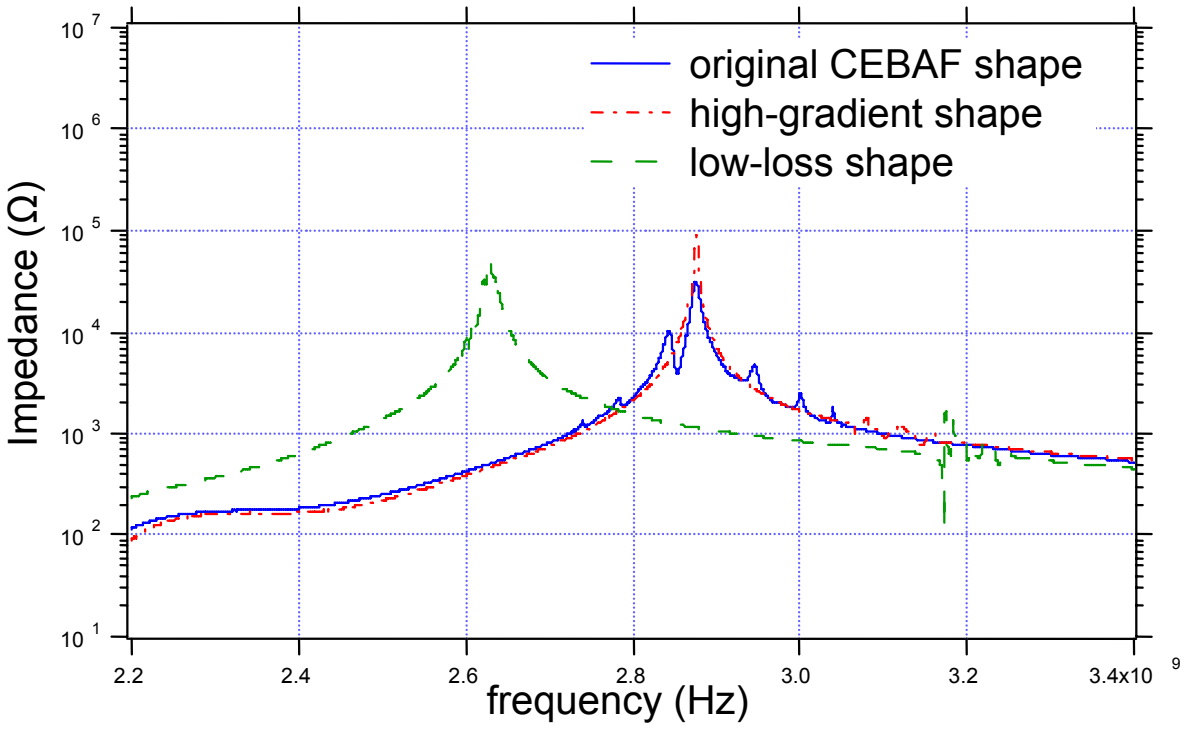
original CEBAF shape
high-gradient shape
low-loss shape
Impedance (Ω)
frequency (Hz)
10 7
10 6
10 5
10 4
10 3
10 2
10 1
2.2
2.4
2.6
2.8
3.0
3.2
3.4x10 9

Figure 16.

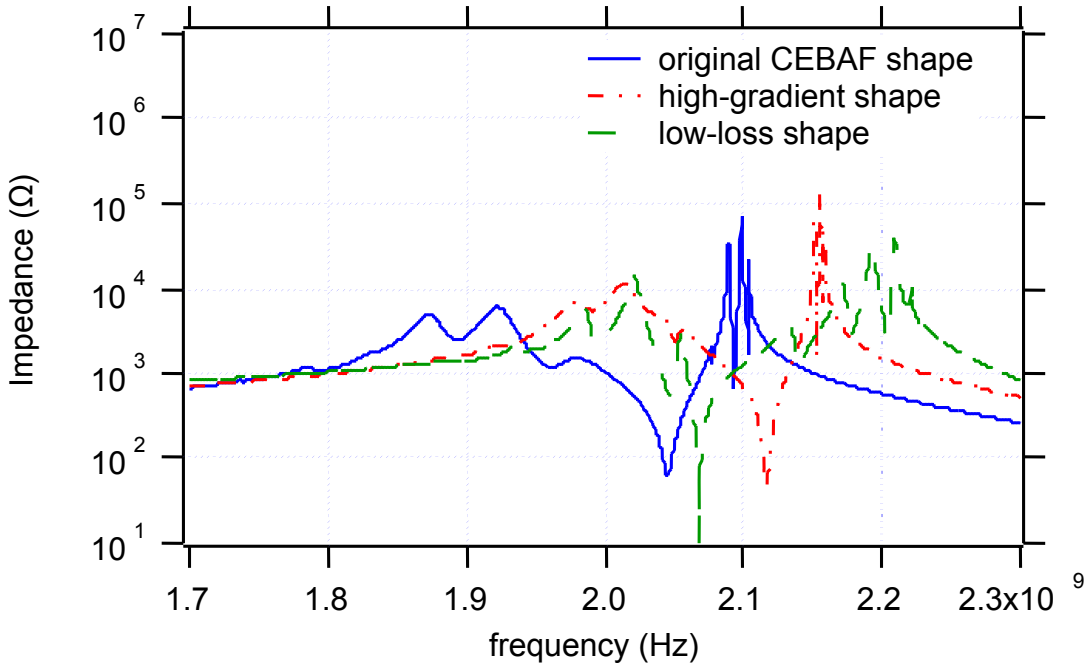
original CEBAF shape
high-gradient shape
low-loss shape
Impedance (Ω)
10 7
10 6
10 5
10 4
10 3
10 2
10 1
1.7
1.8
1.9
2.0
2.1
2.2
2.3x10 9
frequency (Hz)

Figure 17.

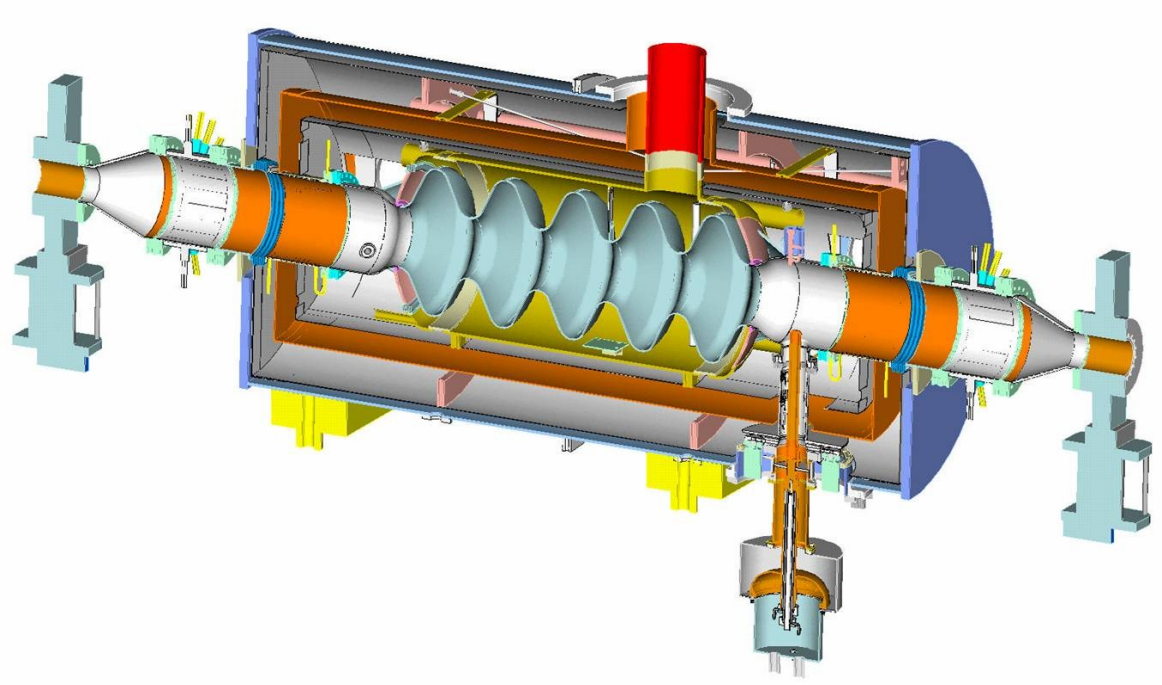

Figure 18.

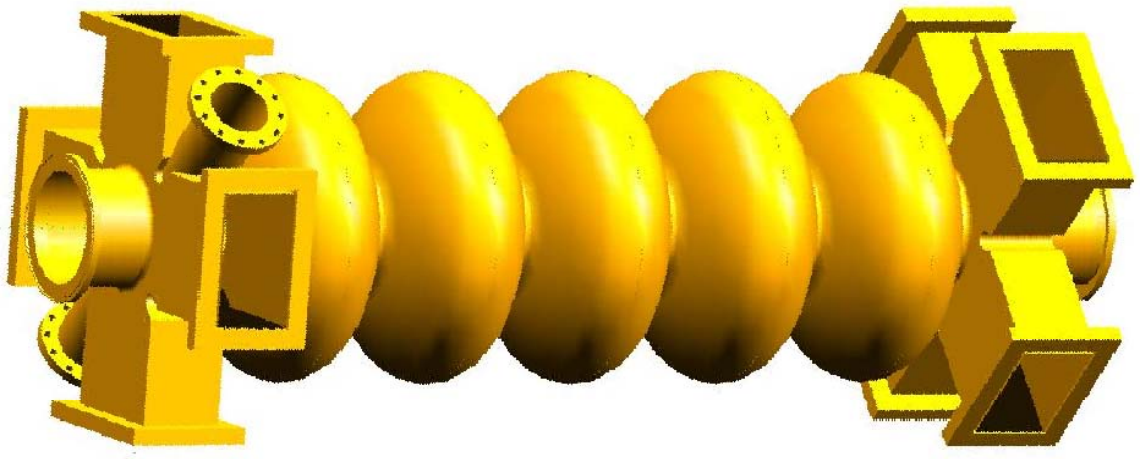

Figure 19.

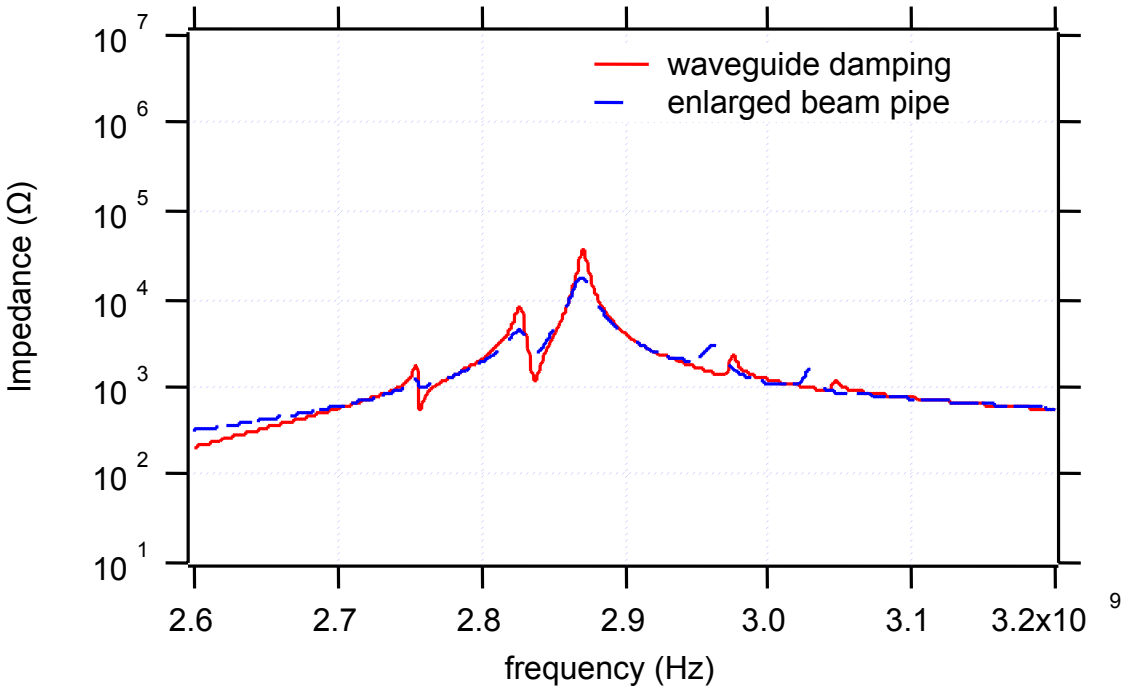
waveguide damping
enlarged beam pipe
Impedance (Ω)
10 7
10 6
10 5
10 4
10 3
10 2
10 1
2.6
2.7
2.8
2.9
3.0
3.1
3.2x10 9
frequency (Hz)

Figure 20.

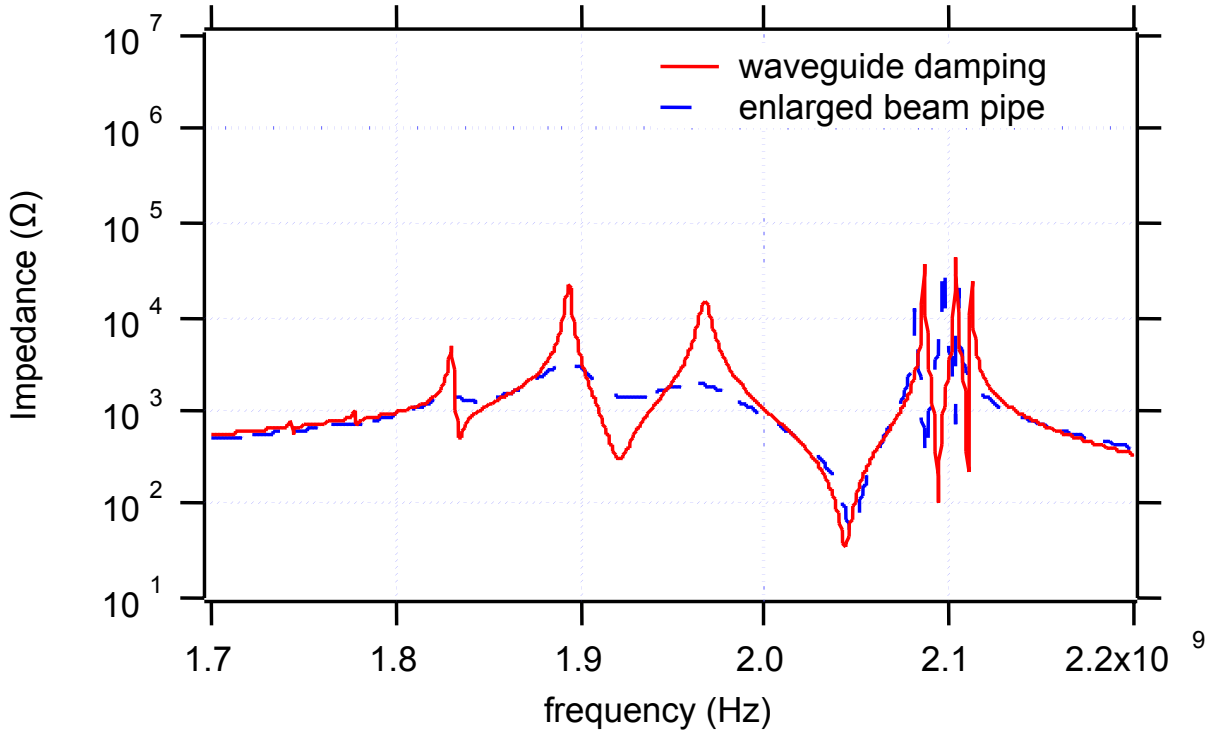
waveguide damping
enlarged beam pipe
Impedance (Ω)
10 7
10 6
10 5
10 4
10 3
10 2
10 1
1.7
1.8
1.9
2.0
2.1
2.2x10 9
frequency (Hz)

Figure 21.

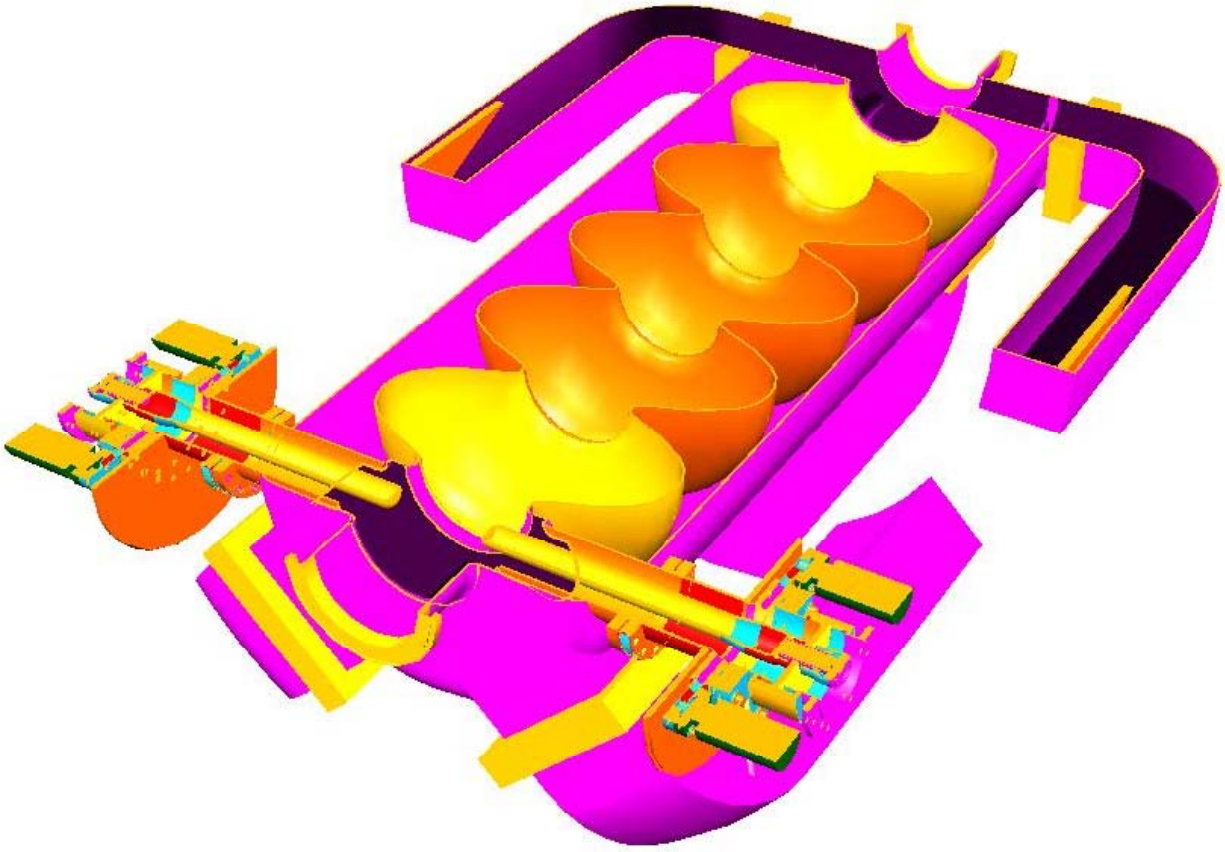

Figure 22.

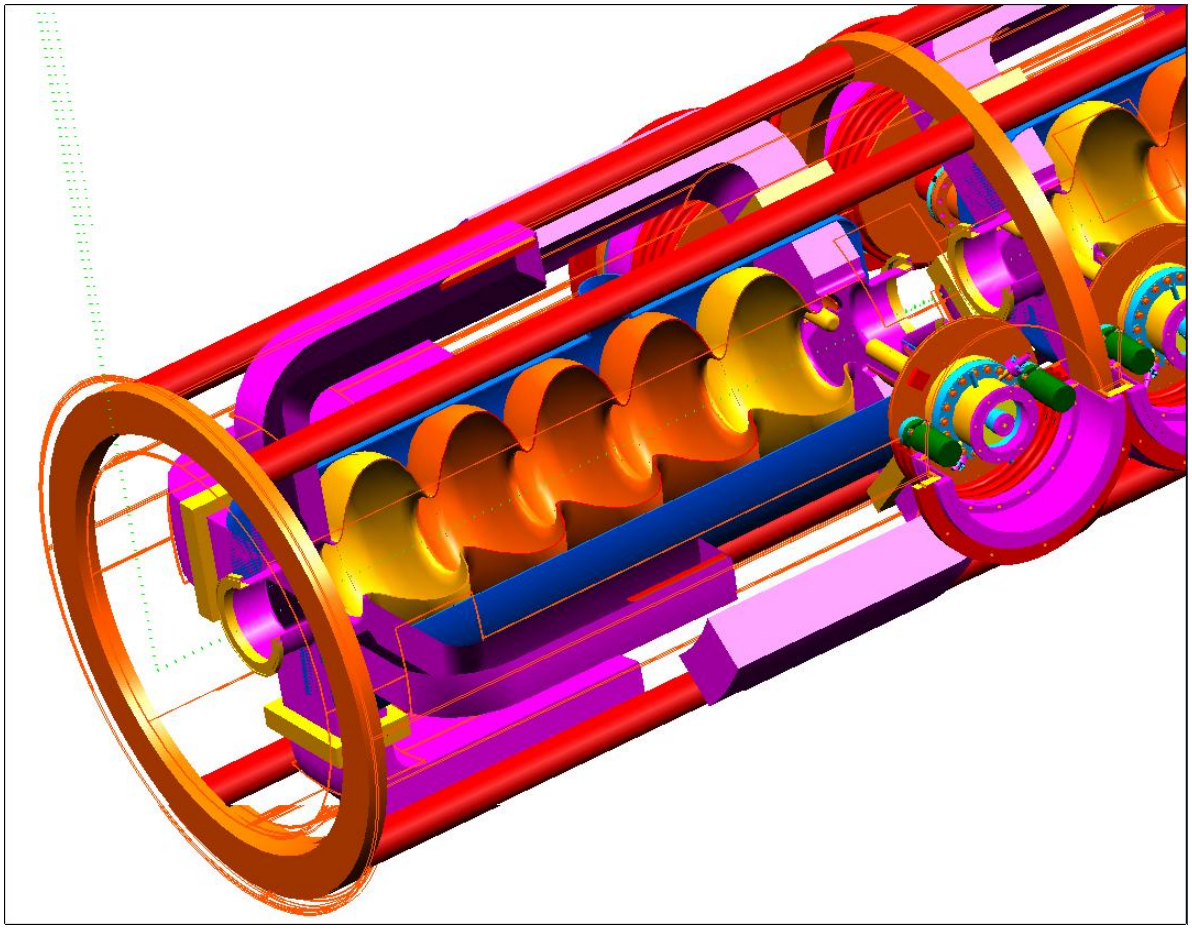

Figure 23.

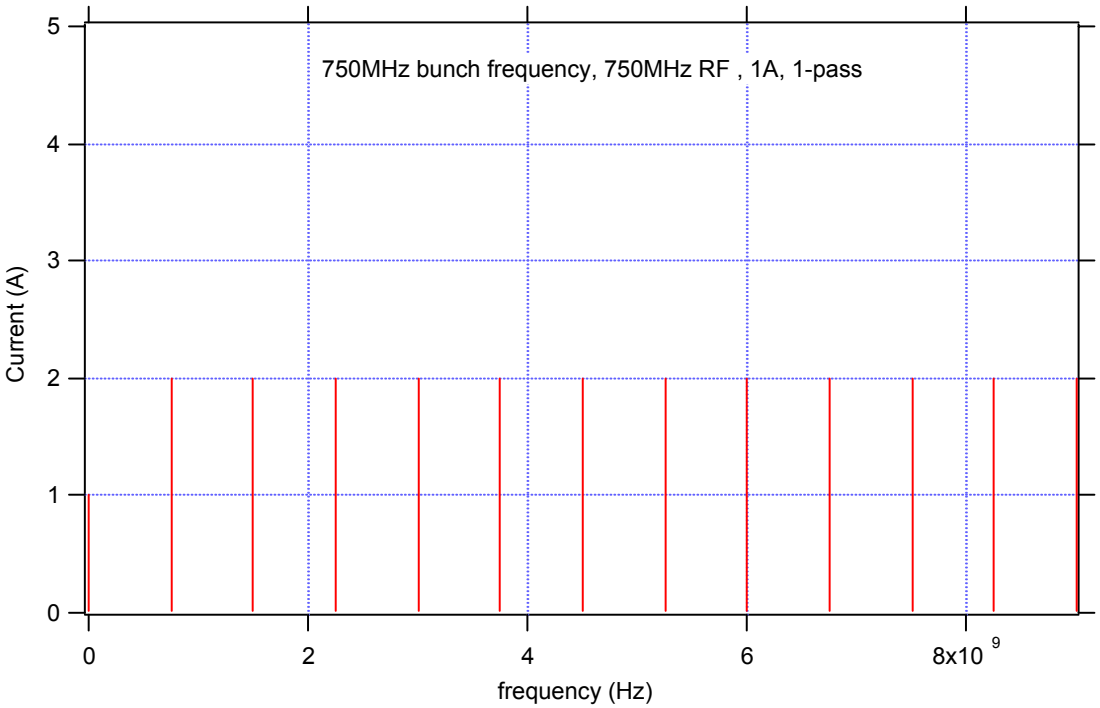
750MHz bunch frequency, 750MHz RF , 1A, 1-pass
Current (A)
frequency (Hz)
0
1
2
3
4
5
0
2
4
6
8x10 9

Figure 24.

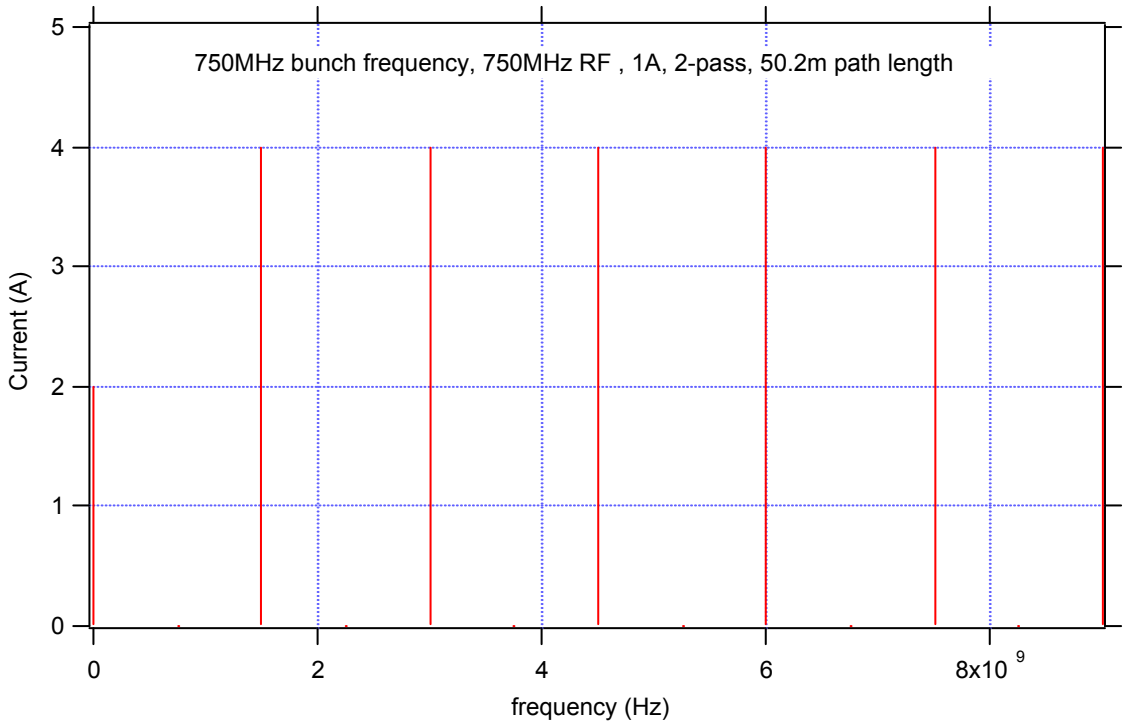
750MHz bunch frequency, 750MHz RF , 1A, 2-pass, 50.2m path length
Current (A)
0
1
2
3
4
5
0
2
4
6
8x10 9
frequency (Hz)

Figure 25.

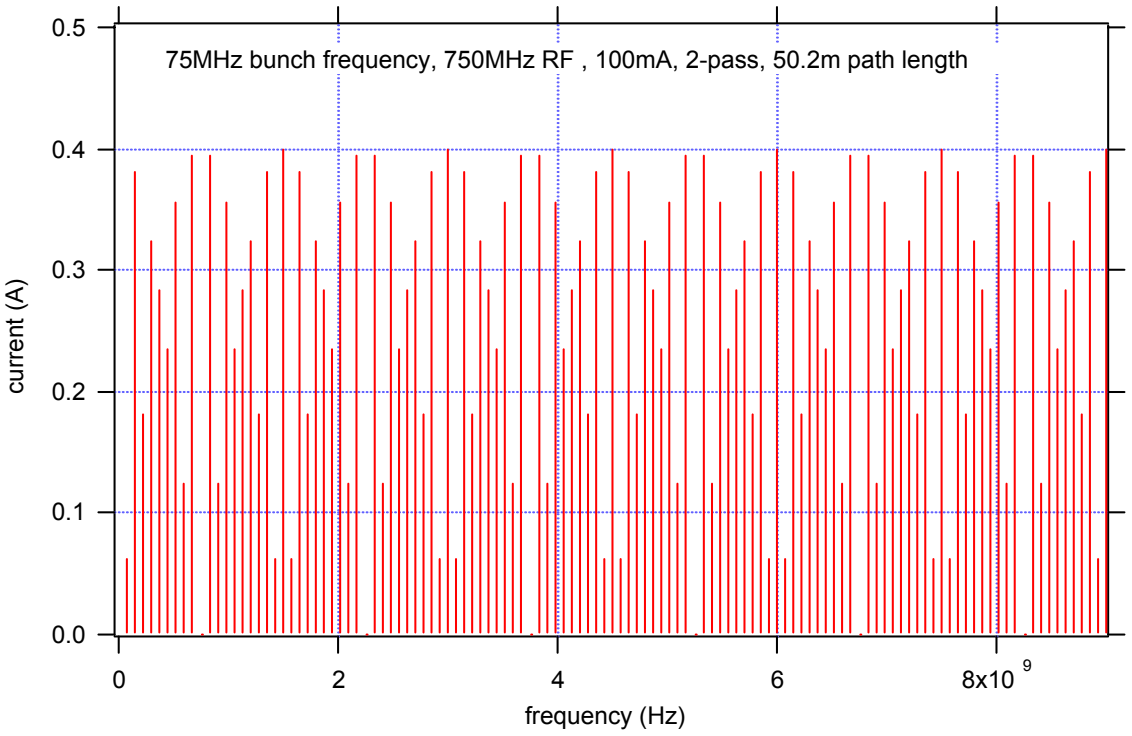
75MHz bunch frequency, 750MHz RF , 100mA, 2-pass, 50.2m path length
current (A)
0.5
0.4
0.3
0.2
0.1
0.0
0
2
4
6
8x10 9
frequency (Hz)

Figure 26.

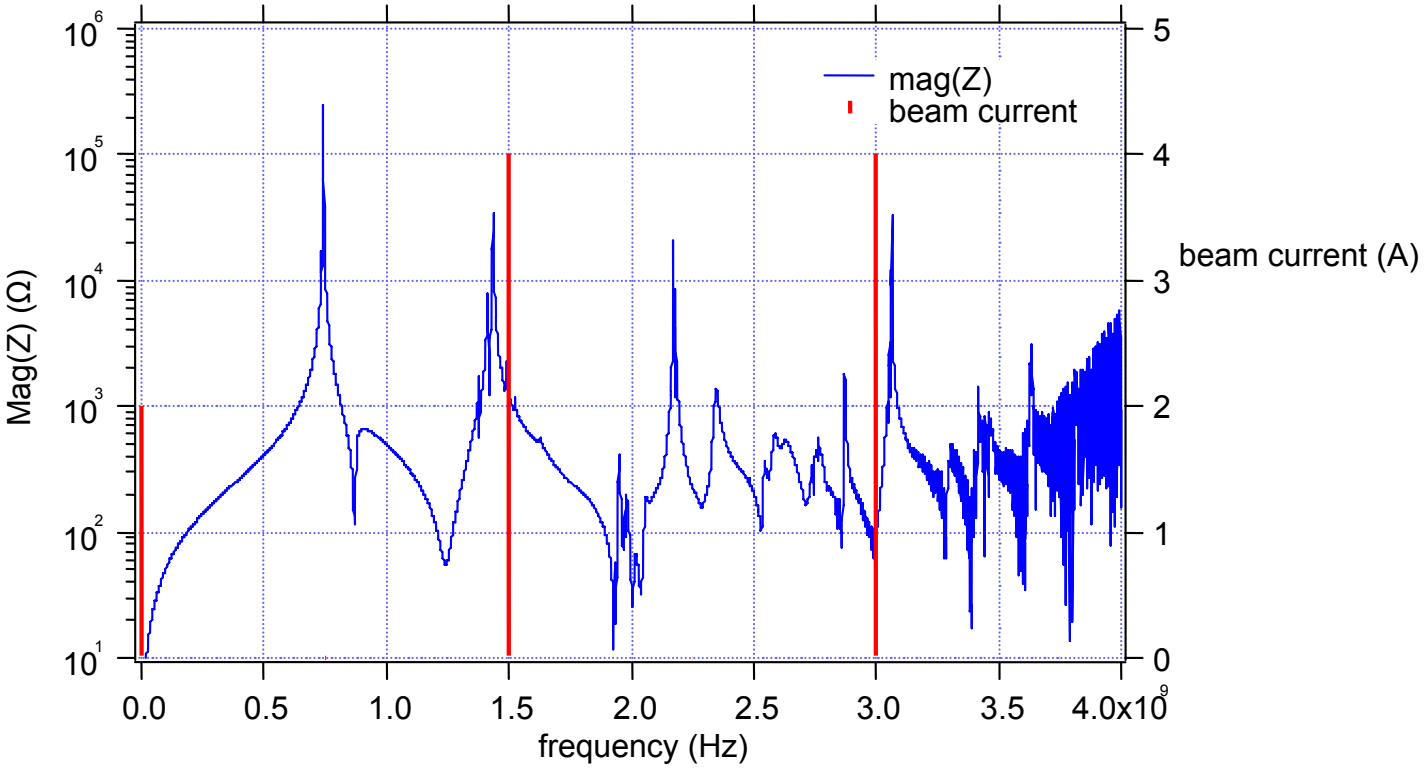

Figure 27.

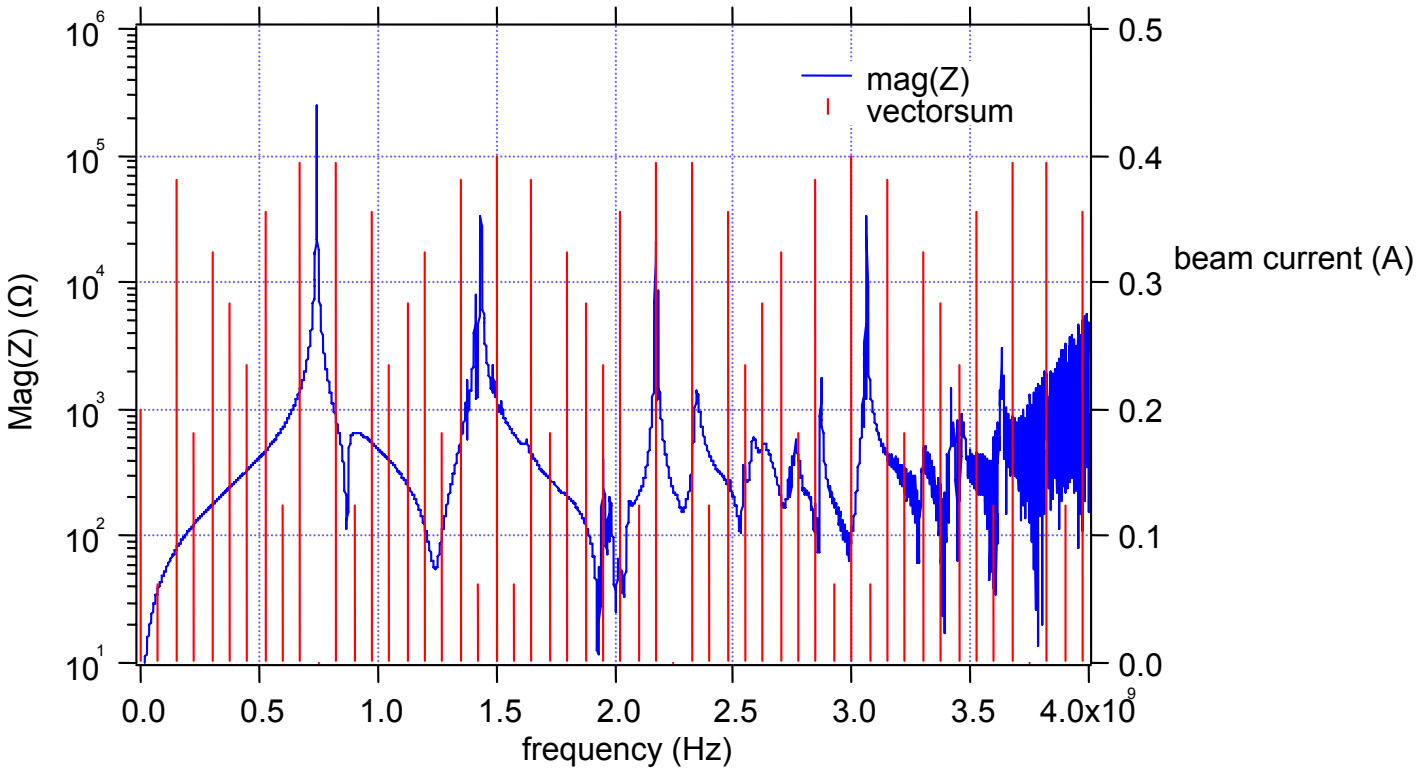

Figure 28.